ACS APPLIED MATERIALS & INTERFACES

Research Article

www.acsami.org

Single-Step Process for the Deposition of High Water Contact Angle and High Water Sliding Angle Surfaces by Atmospheric Pressure Dielectric Barrier Discharge

Nicolas D. Boscher,*[,†] David Duday,[†] Stéphane Verdier,[‡] and Patrick Choquet[†]

[†]Science and Analysis of Materials Department, Centre de Recherche Public - Gabriel Lippmann, Belvaux, L-4422, Luxembourg

[‡]Innovation Centre, Eurofoil Innovation Centre, Eurofoil, Belvaux, L-4422, Luxembourg

ABSTRACT: Fluorine-free surfaces with high water contact angle (WCA) and high adhesion force to water are prepared by the atmospheric pressure dielectric barrier discharge (AP-DBD) of hexamethyldisiloxane on cold rolled aluminum foil. Water droplets, which remained on the plasma-polymerized hexamethyldisiloxane (ppHMDSO) surface with contact angle of 155°, do not slide even when the surface is tilted vertically or turned upside down. Scanning electron microscopy, atomic force microscopy and confocal microscopy highlight the importance of the dual-scale roughness of the ppHMDSO surface. The "sticky" high WCA property is achieved only when the nanometer scale particles generated during the AP-DBD process are present at the surface of the film and combine to the micrometer scale rolling lines of the aluminum substrate.

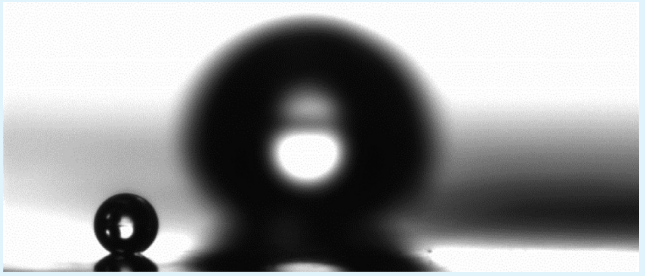

KEYWORDS: *superhydrophobic surfaces, plasma-polymerized hexamethyldisiloxane thin films, atmospheric pressure dielectric barrier discharge, dual-scale roughness, water adhesion*

1. INTRODUCTION

In the past decade, numerous studies have focused on controlling the surface nano- and microstructure to mimic the dual-scale roughness of superhydrophobic lotus leaves or the high water contact angle (WCA) and large water sliding angle (WSA) of rose petals.[1,2] Depending on the size of the micro- and nanostructures, which can both be in the Cassie−Baxter[3] or Wenzel[4] state, four different wetting states are possible, leading to either "slippy" or "sticky" surfaces with high WCA. Through the combination of microscopic cells (3−11 μm diameter and 7−13 μm height) and nanoscopic wax crystals (100 nm),[5] the leaves of the lotus flower exhibit high WCA and low WSA that give rise to the self-cleaning behavior of the plant.[6] The water droplets, which do not penetrate the interstitial porosities formed by the micro- and nanostructures (Cassie−Cassie's state),[3] easily roll off of the lotus leaves. In contrast, despite forming heterogeneous contact with the nanofolds (730 nm) present at the surface of the rose petals, water droplets are allowed to impregnate the microstructure formed by large micropapillaes (16 μm diameter and 7 μm height), leading to a surface with high WCA and high adhesive force to water (Wenzel-Cassie's state).[7] The droplets, which remain spherical in shape on the petal surface, do not roll off even if the petal is turned upside down.

Surfaces with both high WCA and high WSA, which may be useful for microfluidic devices,[8] have drawn a growing interest in recent years.[9] The first such surface was prepared from anodized alumina templates to form aligned polystyrene nanotube layers.[1] Because other fluorine-free high WCA and high WSA materials involving multistep processes have also been reported, such as shear-controlled micro- and nanometer-scaled isotactic polypropylene surfaces[10] or spin-coated polydimethysiloxane (PDMS) vinyl terminated onto etched aluminum templates.[11] However, the great majority of such surfaces has been deposited from fluorinated monomers[2,12] or prepared by the fluorination of various nanostructured surfaces[13,14] such as femtosecond laser irradiated silicon[15] or spin-coated silica nanoparticles onto patterned substrates.[16]

Among the different materials cited to prepare superhydrophobic surfaces, PDMS has been widely studied. PDMS consist of a siloxane skeleton (−Si−O−) linked to two methyl groups, which are responsible for the nonpolar and hydrophobic character of this optical transparent polymer. Nanopillar arrays, vessels or rough surfaces of this low surface energy polymer have been formed by soft lithographical replication of a template,[17] spin-casting onto a mold,[18] toluene extraction of a methylsilicone network,[19] laser etching,[20] and aerosol assisted chemical vapor deposition.[21] The atmospheric pressure plasma polymerization of organosilicon precursors has also allowed the growth of superhydrophobic polysiloxanes coatings with low water contact angle hysteresis.[22−24] Notably, plasma-polymerized hexamethyldisiloxane (HMDSO) superhydrophobic thin films have been deposited thanks to a remote radio frequency (RF) plasma jet operating in helium[22] or argon.[23] The dielectric

Received: November 21, 2012
Accepted: January 22, 2013
Published: January 22, 2013

barrier discharge plasma deposition of hexamethylcyclotrisiloxane (HMCTSO) has also allowed the growth of superhydrophobic polysiloxanes coatings with low water contact angle hysteresis.[24] However, the double rough structure, grown thanks to a nonequilibrium filamentary DBD, was reported as very soft and weak. Over the past five years, the atmospheric pressure (AP)-DBD deposition of organosilicon films has attracted a lot of interest, mainly for anticorrosion and adhesion purposes.[25] AP-DBD is an environmentally friendly technology, which does not imply the use of solvent and bath nor the production of large amount of unwanted byproducts and wastes. Moreover, it can operate at room temperature, does not require heating nor vacuum devices, and can be easily adapted on a coil-to-coil production line.[26]

In this paper, we present a single-step process to the large-scale production of fluorine-free surface with both high WCA and high adhesion force to water. The "sticky" high WCA ppHMDSO films were deposited on aluminum foil by the AP-DBD reaction of HMDSO in nitrogen atmosphere. The chemical composition of the coatings, with a WCA as high as 155°, was characterized by Fourier-transform infrared spectroscopy (FTIR) and X-ray photoelectron spectroscopy (XPS). The morphology of both the substrate and the film were investigated by scanning electron microscopy (SEM), confocal microscopy and atomic force microscopy (AFM). It will be shown how the association of the microroughness of the cold-rolled aluminum foil and the nanoscale roughness created during the plasma deposition process led to the formation of high WCA ppHMDSO thin films with high adhesion properties to water.

2. EXPERIMENTAL SECTION

2.1. Plasma-Assisted Deposition and Materials. The AP-DBD reactor used in this study was constituted of two flat parallel high voltage electrodes (2 × 1.5 × 30 cm^2) covered with alumina and a moving stage as grounded electrode (10 mm s^{-1}). The process used a high voltage alternating current (10 000 or 22 500 Hz) with a constant dissipated power of 100 W (1.1 W cm^{-2}) generated by a Corona generator 7010R from SOFTAL electronic GmbH. The organosilicon precursor, hexamethyldisiloxane (HMDSO), was injected into the reactor using a classic bubbler system made of a cylinder and a frit. The respective flow rates of nitrogen through the process gas line and the HMDSO bubbler were kept constant to 19.5 and 0.5 L min^{-1} (1000 ppm), respectively, for all experiments. The aluminum substrates, typically of DIN-A4 size, were 200 μm thick foils of a 8011 alloy with different roughnesses − cold-rolled aluminum foil or polished aluminum foil. The arithmetic average of the absolute deviation from the mean line of all points of the profile (R_a) and the arithmetic average of the five biggest maximum peak-to-valley heights (R_z) were measured as 0.18 and 0.89 μm for the rougher substrate and 0.06 and 0.40 μm for the polished one. The cold rolled aluminum foils were polished using a Mecapol P200 polishing machine with silicon carbide discs (P2400, P1200, P800, P400) and Reflex pad polishing cloths (STA 6 μm, RAM 3 μm, TFR 1 μm). The substrates were cleaned by a 60 s exposure to an N_2:O_2 (95%: 5%) AP-DBD plasma. The precursor, HMDSO, was obtained from Sigma-Aldrich and used without further purification (98%). N_2 (99.999%) gas was obtained from Air Liquide. The deposition time was 60 s for all the experiments.

2.2. Surface Characterization. The water contact angle (WCA) of the films and the pictures of the droplets were obtained using a Krüss DSA16 EasyDrop USB contact angle meter. The size of the deionized water drop used for the measurements was 3 μL. The contact angle measurements were consistent across the whole coated substrate, and did not change over a period in excess of one year, due to the chemical stability of the coatings. The advancing (ACA) and receding contact angles (RCA) measurements were performed starting with a 3 μL droplet which was slowly increased to 10 μL and decreased to 3 at 0.5 μL s^{-1}. Solutions of different pH values were used to investigate the pH dependence of the wettability properties of the films formed. The acidic and alkaline solutions were respectively prepared from hydrogen chloride and sodium hydroxide.

Fourier-transform infrared analyses (FTIR) were performed on a Bruker IFS 66 spectrometer equipped with a Specac Golden Gate diamond ATR accessory. Three spectra were acquired on a ∼1 mm^2 area for each sample. All three spectra were identical for each experiment presented here. X-ray photoelectron spectroscopy (XPS) and Auger electron spectroscopy (AES) were carried out using a Thermo Electron Microlab 350 instrument. XPS was performed with a nonmonochromated Al Kα X-ray source ($h\upsilon$ = 1486.6 eV) at a pass energy of 20 eV. Argon sputtering operating at 3 keV and 2 μA was used for approximately 300 s in a rastering mode in order to remove surface contamination. No flood gun was used to reduce sample charging. Charge calibration was accomplished by fixing the binding energy of the aliphatic carbon at 285 eV. The XPS spectra were fitted by CasaXPS software and a Shirley-type background was subtracted. The Auger analyses were used to study the morphology and the elemental composition of the surface. The lateral resolution achieved was 100 nm with a depth information of a few monolayers. All spectra were recorded in direct mode and with a 10 keV and 1 nA primary beam. The angle of incidence of the primary electrons beam and of escaping electrons was 60° with respect to the surface normal.

Scanning electron microscopy (SEM) was performed on a Leica Stereoscan 430i (LEO). Surface morphology of ppHMDSO coated aluminum surfaces were examined on a micrometer scale using atomic force microscopy (AFM) and on a micrometer scale using confocal microscopy. Different areas were studied on each sample in order to obtain representative data. The AFM images were recorded in tapping mode by a Molecular Imaging PicoSPM LE, using a 100 μm scanner and scan rate of 1 Hz/line. The AFM image covers an area of 5 × 5 μm^2. Confocal microscopy was carried out with a NanoFocus MicroSurf 3D confocal white light microscope (NanoFocus AG, Germany). Using the 20× magnification lens, the confocal image covers an area of 800 × 800 μm^2 with a pixel resolution of 512 × 512.

3. RESULTS AND DISCUSSION

3.1. Fabrication of ppHMDSO Films with High Water Contact Angle and High Adhesion Force to Water. Figure 1 illustrates a scheme of the AP-DBD reactor used for the fabrication of ppHMDSO surfaces with both high WCA and high adhesion force to water. The aluminum substrate (DIN-A4 size), placed on a moving table acting as grounded electrode, was exposed to an atmospheric pressure plasma discharge generated when passing under high voltage electrodes. Regardless of the substrate roughness or plasma frequency, the plasma, fed with nitrogen and 1000 ppm of the precursor (HMDSO), operated in the filamentary mode and led to the formation of transparent films, without any crack observed on the surface and almost indistinguishable from each other. The growth rate, determined from the measured thicknesses using a contact profilometer, was 8 nm s^{-1} for all the different conditions investigated. A linear dependence between the thicknesses of deposited films and the deposition time was observed.

The WCA on the ppHMDSO thin films was observed to be strongly dependent on the aluminum substrate and the plasma frequency (Table 1). While films deposited on polished aluminum foil or at a plasma frequency of 10, 000 Hz exhibited WCA with values in the range 98−106° (Figure 2a), films deposited on cold-rolled aluminum foil at a plasma frequency of 22 500 Hz were highly hydrophobic with WCA as high as 155°. Surprisingly, tilting experiments show that despite their high water contact angle, small water droplets clung to the surface

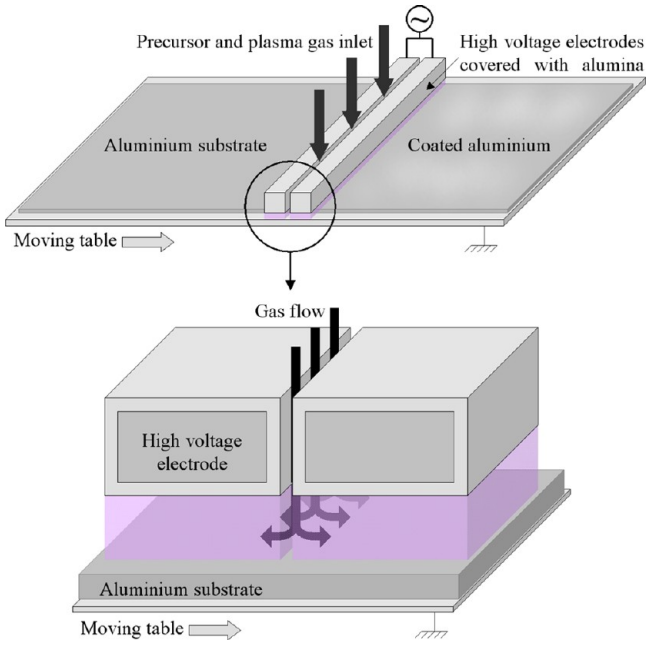

Figure 1. Schematic of the AP-DBD reactor used for the fabrication of the ppHMDSO films with high WCA and high adhesion force to water.

Table 1. Water Contact Angle, Advancing, and Receding Contact Angles of the Siloxane Films Produced for the Different Frequencies and Substrate Roughness

frequency (Hz)	aluminum substrate	WCA (deg)	ACA (deg)	RCA (deg)	CAH (deg)	WSA (deg)
10 000	polished	98	108	77	31	>90
10 000	cold-rolled	106	115	79	35	>90
22 500	polished	103	110	83	31	>90
22 500	cold-rolled	155	171	138	33	>90

(Figure 2b) and a large water contact angle hysteresis (ca. 33°), with an advancing and receding contact angles of 171° and 138°, respectively, was observed. The spherical water droplets did not roll off nor slide on the ppHMDSO coating, even when the surface was tilted at 90° or turned upside down. However, this effect failed for water droplets larger than 5 μL because the drop's weight overcomes the adhesion forces of the ppHMDSO films. After 1 year storage in air, new WCA and WSA measurements matched the observations made just after the film preparation, indicating the high chemical stability of the deposited films coatings. It can also be highlighted that even after immersion in water or ethanol, the layers did recover their high WCA properties after drying.

Figure 3 shows the relationship between the pH values of the aqueous solution and the CA. No obvious fluctuation was observed in the pH range from 2 to 14 with all CA values in the range from 151 to 158°. The CA measured for the most acidic droplets (pH value of 1) was only 145°. Moreover the droplet was observed to slowly spread on the surface, to reach a CA of 120° 2 min after the first measurement. This was not observed for all the other pH values investigated as the droplets evaporated before any change in the CA was noticed. The high stability of the HMDSO films produced by AP-DBD has already been reported in previous studies.[27,28] Such surfaces could find applications for manipulating tiny quantities of biological liquids or corrosive liquids, which have to be held in place without leaking or being contaminated by nearby materials.

3.2. Chemical Characterization of the ppHMDSO Films. Fourier transform infrared spectroscopy (FTIR) confirmed the reticulation of ppHMDSO thin films (Figure 4).[28,29] All the spectra, irrespective of the plasma electrical excitation frequency or substrate roughness, were almost identical with a broad and intense band between 1000 to 1200 cm^{-1} and a narrow peak at 1260 cm^{-1}. These peaks were respectively assigned to different Si−O−Si chain vibrations and Si-$(CH_3)_2$ bending modes. The intense bands observed between 700 and 900 cm^{-1} were attributed to vibrations from Si−O−Si (736 cm^{-1}), Si-$(CH_3)_1$ (778 cm^{-1}), ρ (CH_3) and ν (Si−C) from Si-$(CH_3)_3$ (764 cm^{-1} ;830−850 cm^{-1}), Si-$(CH_3)_2$ (800 cm^{-1}; 904 cm^{-1}), δ (Si−O) (810−849 cm^{-1}) and δ ((H−Si−O) (848 cm^{-1}; 890 cm^{-1}). Around 1400 and 2900 cm^{-1}, peaks with shoulders corresponding to asymmetrical CH_3 deformation vibrations and CH_3 stretching modes were observed. The weak peaks at 1555 and 1655 cm^{-1} demonstrate the existence of C═N (sp^2) bonds in all the films deposited. The presence of C−N (sp^3) bonds, identified by XPS, could not be clearly confirmed as its contribution (1200 cm^{-1}) was hidden by the strong Si−O−Si chain vibrations peak.

X-ray photoelectron spectroscopy (XPS) showed that the chemical composition of the films was not influenced by the plasma frequency or the substrate roughness. All the layers had an almost identical composition with 27, 24, 41, and 8% silicon, oxygen, carbon, and nitrogen, respectively. Auger electron spectroscopy showed no disparity between the stoichiometry of the films and the particles observed on their surface. The chemistry of the silicon based units in the films was determined following a methodology based on the XPS curve-fitting of Si 2p, C 1s, O 1s, and N 1s core levels.[30,31] The Si 2p peak was fitted with a sum of four components corresponding to the main four different silicon environments present in the HMDSO coating: $[(CH_3)_3SiO_{1/2}]$ or M, which forms only one bond with the rest of the matrix and corresponds to a chain terminating group; $[(CH_3)_2SiO_{2/2}]$ or D, which is a chain propagating unit, $[(CH_3)_1SiO_{3/2}]$ or T and $[SiO_{4/2}]$ or Q, which are chain-cross-linking units. The four Si 2p components, for which the binding energies are known and gradually increase for the replacement of each methyl group by an additional oxygen atom, were linked in area and binding energy to their respective C 1s and O 1s components. The peak positions and fwhm were obtained both from the literature[30−32] and calibration measurements made from PDMS and SiO_2. The Si 2p, C 1s, O 1s, and N 1s peaks were all fitted together by constraining the shift in binding energy between all the different components, keeping a fwhm identical for all the components of a same peak and the appropriate area relations between the different components of a same siloxy unit. The curve-fitting of the Si 2p core level showed that all the films deposited were mainly composed of $[(CH_3)_2SiO_{2/2}]$ siloxy unit (ca. 68%), which correspond to the PDMS structure with a hydrophilic Si−O backbone along with hydrophobic methyl pendent groups (Figure 5). Neither the substrate roughness nor the plasma frequency was found to influence the concentrations of the different siloxy units contained in the films. The respective concentrations of the four possible siloxy units in the films, M, D, T, and Q units, were calculated as follow: 6, 68, 17, and 9% for the films deposited from a 22 500 Hz electrical excitation frequency.

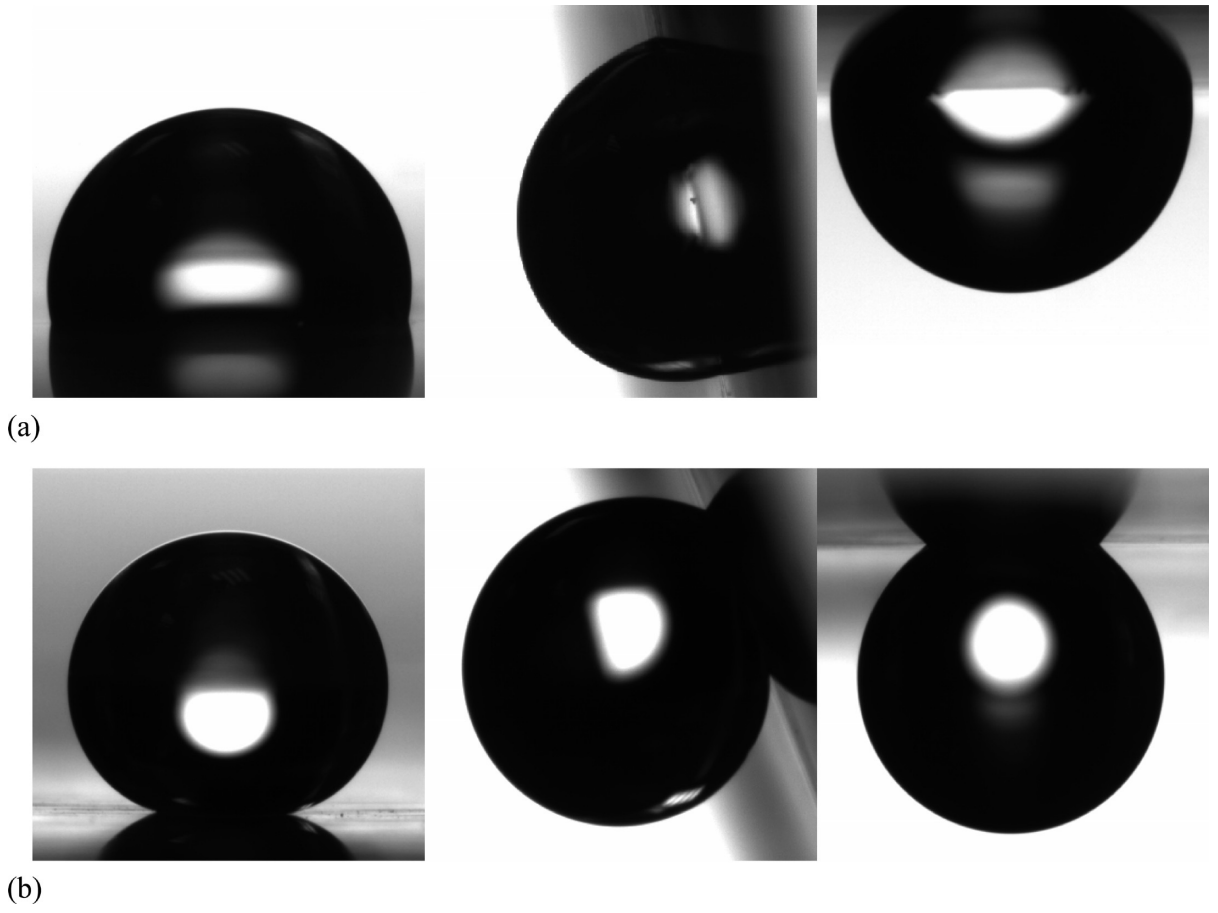

Figure 2. Water droplets (3 μL) on the ppHMDSO coated cold-rolled aluminum foil for different plasma frequencies: (a) 10 000 and (b) 22 500 Hz. Left: water droplet on a film at 0° tipping angle; middle: water droplet on a vertically oriented substrate; right: water droplet suspended upside down on the substrate.

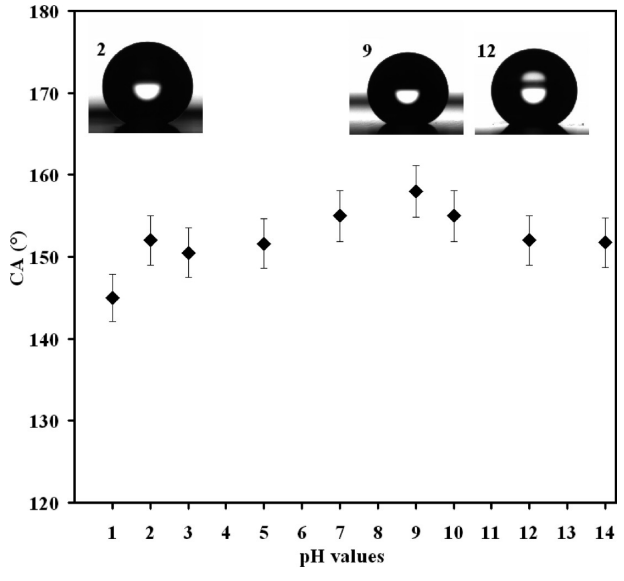

Figure 3. Contact angle as a function of the pH values.

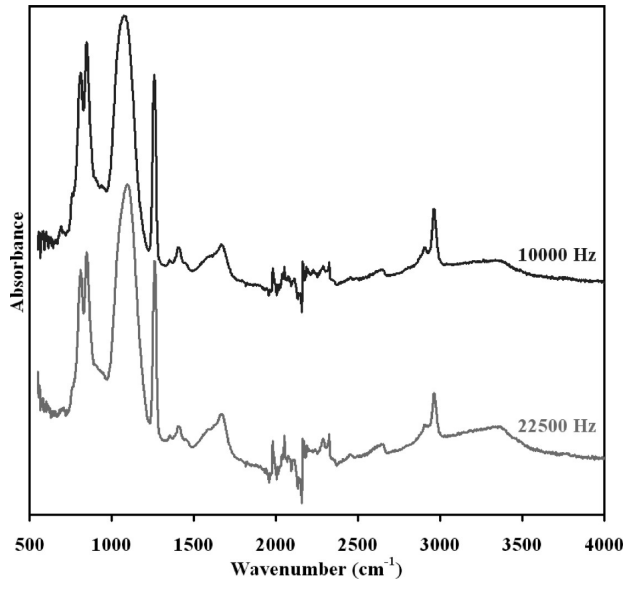

Figure 4. FTIR spectra of the films deposited at room temperature with a 10 000 Hz and 22 500 Hz frequencies.

The chemical composition of the layers being shown to be independent of the substrate roughness and plasma electrical excitation frequency, the surface energy of the surface was determined for the coating deposited on smooth aluminum substrate using the 10 000 Hz frequency. The contact angle of three different solvents, water (98°), ethylene glycol (78°), and diiodomethane (66°), for which the different surface energy components are known, led to a total surface energy of 25 mJ m^{-2}. The dispersive and polar components were evaluated to

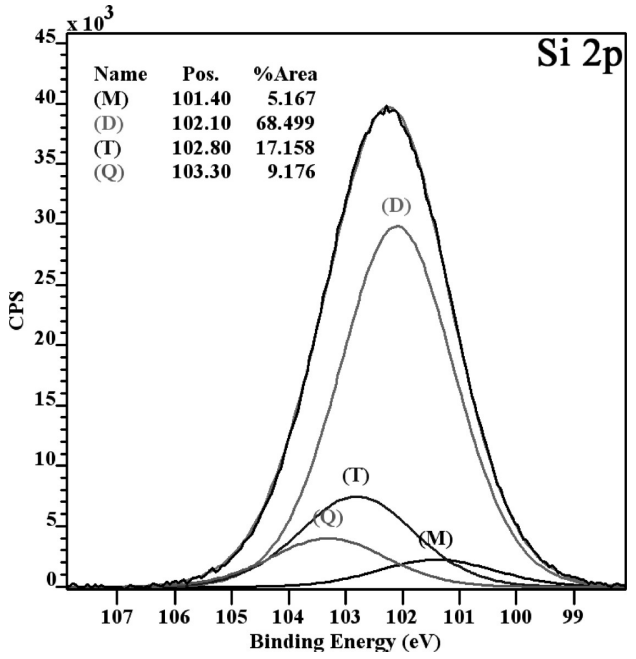

Figure 5. XPS curve-fitting of the Si 2p core level of the films deposited at 22 500 Hz.

24 and 1 mJ m^{-2}, respectively, and are quite comparable to the reported values for PDMS.

3.3. Micron and Nanometer Length Scales of the High WCA ppHMDSO Surfaces. FTIR and XPS analyses showed that the large differences observed in the measured WCA were not related to any chemical disparity between the films produced. It is well-known that the roughness or texture of a film can influence the WCA at its surface.[3,4] The reported WCA for a smooth PDMS surface is 105°.[33] While the highest WCA measured on a flat surface is only 119° and is achieved with hexagonal close aligned $-CF_3$ groups.[34] Above this value, any increase of the WCA is due to the surface topography.[35,36] The presence of roughness and in particular of multiscale roughness is essential to achieve surfaces with WCA greater than 150°.[37] Therefore, the high contact angles of the films prepared here suggest extreme roughness, which is confirmed by the SEM pictures of the films deposited at 22 500 Hz on the cold rolled aluminum foil (Figure 6a). At low magnification (× 1000), the films deposited at 10 000 Hz and 22 500 Hz on the cold-rolled aluminum foils were indistinguishable from each other (Figure 6a, b). The SEM pictures of these films showed rolling lines due to the cold rolling process of the aluminum foil. Pinholes surrounded by numerous particles, with a size distribution varying from 200 to 300 nm, were also observed at their surface. The use of a 1 mm gap at atmospheric pressure and the high precursor concentration imply that the nitrogen plasma discharge operates in the filamentary mode.[38] The filaments (current channels), electron and ion bombardment, yield to the formation of pinholes and heterogeneities in the films. As observed on the SEM micrographs, in the early steps of the deposition process, the filaments preferentially anchored to surface defects and in particular to the rolling lines. Moreover, etching of the surface under the impact of the filaments induced a high concentration of condensable vapors, which quickly generated numerous particles associated with holes. The local higher power density at the filament position also induced a faster gas depletion and nucleation of particles.[39] In contrast,

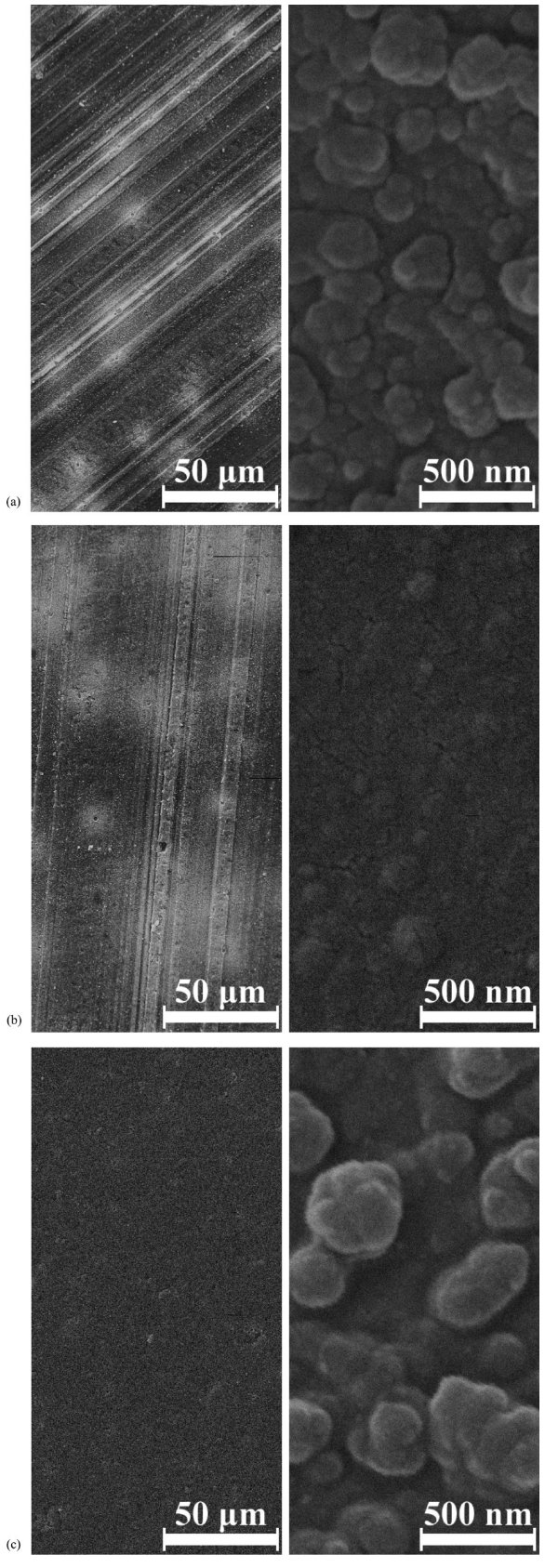

Figure 6. Scanning electron micrographs of the films produced on a cold-rolled aluminum foil at plasma frequencies of (a) 22 500 and (b) 10 000 Hz and (c) on a polished aluminum substrate at a 22 500 Hz plasma electrical excitation frequency.

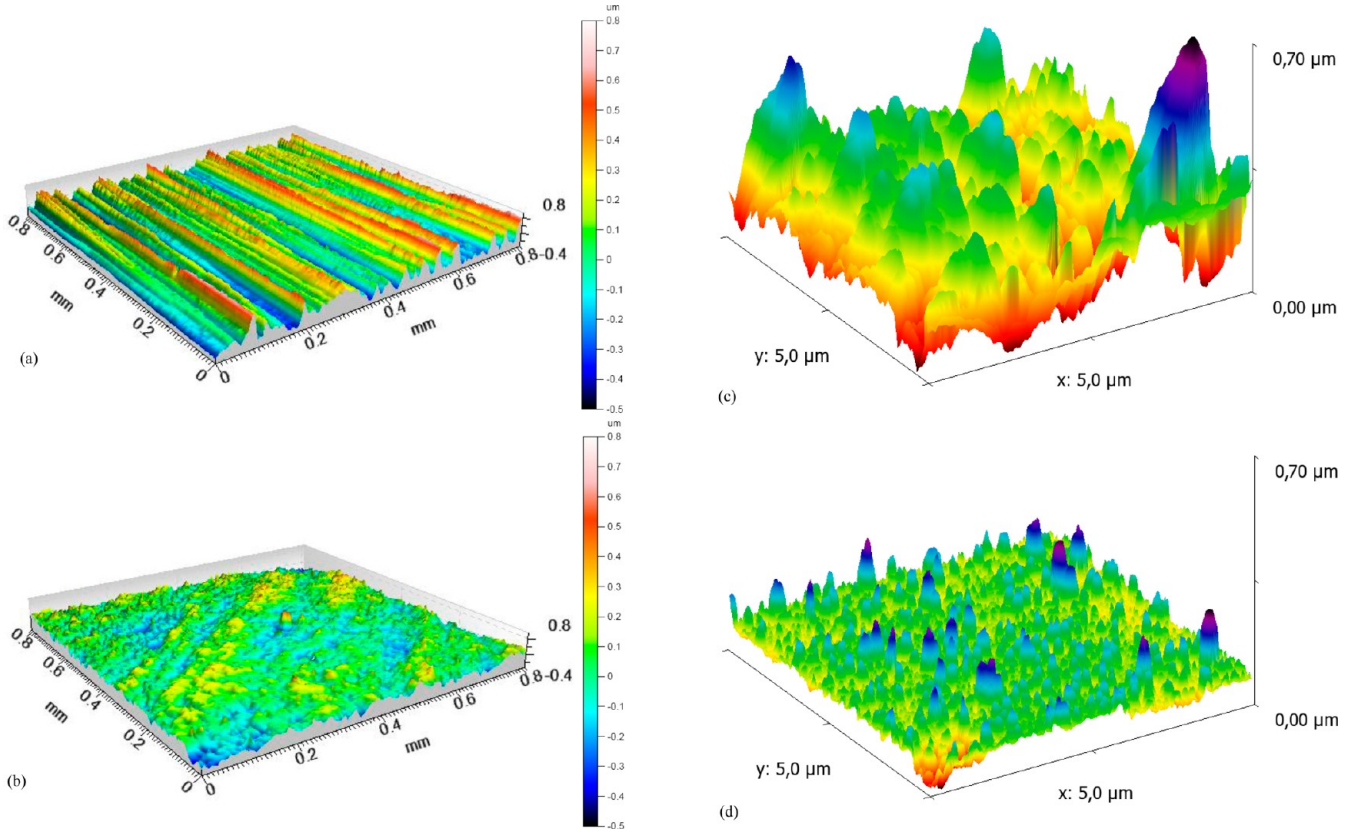

Figure 7. Confocal microscopy 3D topographic images of the films deposited with a 22 500 Hz frequency on (a) cold-rolled and (b) polished aluminum foil. Atomic force microscopy 3D topographic images of the films deposited with (c) a 22 500 Hz frequency and (d) a 10 000 Hz frequency on the cold-rolled aluminum foil.

the films deposited from either frequency on polished aluminum foil were observed to be relatively smooth and seemed to be particle-free at low magnification (Figure 6c). High-magnification SEM pictures (×100 000) revealed that the films deposited using a 22 500 Hz frequency on cold-rolled or polished aluminum substrates were composed of agglomerated particles (Figure 6a, c). Although these particles, with sizes varying from 200 to 300 nm, were constructed from smaller agglomerated primary particles (ca. 50 nm), the films deposited at 10 000 Hz had a smoother appearance, with weaker evidence of particle formation at high magnification (Figure 6b).

The micrometer and nanometer scale roughnesses observed by SEM were respectively characterized by confocal microscopy and atomic force microscopy (AFM). Confocal microscopy of the coated and uncoated cold-rolled aluminum foils, irrespective of the plasma frequencies or the deposition temperature, revealed the same feature with long parallel rolling lines that covered the whole surface of the samples (Figure 7a). The observed rolling lines are due to the topography transfer of the work rolls during the rolling process of the aluminum foil. The 3D topographic images of the coated and uncoated polished aluminum foil showed a smoother surface, only covered by several smaller peaks (Figure 7b). The size of the rolling lines observed on the roughness profile of the films prepared on the cold-rolled aluminum foil (Figure 7a), with an average width and height of 10 and 1 μm, respectively, is consistent with the scale of the microscopic cells at the surface of the lotus leaf (3−11 μm diameter and 7−13 μm height) and the micropapillae of the rose petal (16 μm diameter and 7 μm height). When referring to these values, it can be noticed that as the micropapillae observed on the rose petal, the rolling lines on the aluminum foil are wider than higher. For such low microstructures, the Cassie's state is likely to not be maintained for the base microstructure, implying that water droplets are allowed to impregnate the large furrows, giving rise to the sticky behavior of the high WCA layer. It can also be highlighted that the micrometric pinholes observed at the surface of the films may contribute to the high adhesion of water droplets.

The micrometer roughness observed on the films deposited on the cold-rolled aluminum foils is a condition, but not a sufficient one to achieve surfaces with high WCA. The micrometer scale roughness previously observed by SEM was characterized by AFM. Tridimensional images of films obtained from both frequencies studied were compared with the same vertical scale (Figure 7c, d). The AFM 3D topographic images of the films deposited at 22 500 Hz, irrespective of the aluminum substrate roughness, showed a larger surface roughness than the one of the films deposited a 10 000 Hz. The scale of the ppHMDSO particles at the surface of the films, with an average width and height in the 100 and 200 nm range, is consistent with the size of the nanoscopic wax crystals of the lotus leaf (100 nm),[5] whereas the roundness of the particles and the chink at their surfaces are quite comparable to the structure of the petal rose surface.[7] Confocal microscopy and AFM emphasized the importance of the dual-scale roughness as high water contact angles were achieved only when micrometer scale features in addition of the micrometer features was constructed.

3.4. Plasma Frequency and Formation of Rough ppHMDSO Surfaces. Combination of the cold-rolled aluminum foil microroughness and the film nanoroughness is essential to achieve the desired high water contact angle. The latter is obtained by combining a relatively high precursor concentration (1000 ppm) with a specific plasma excitation frequency (22 500 Hz). It is the mechanism of polymer agglomeration that occurs during the DBD process that is the key to yielding such specific rough surfaces. The relatively high concentration of HMDSO used (1000 ppm) is known to favor the formation of particles in the gas phase,[40] which in turn induces the formation of a large amount of condensable species by the reaction with the reactive species produced by each filament of the AP-DBD. The high concentration of condensable species leads to high local concentration of nucleated particles, which grow by condensation and coagulation.[39,41] The number of formed particles in the gas phase and at the surface of the film is therefore related to the precursor concentration, but also to the density and energy of the filaments of the AP-DBD. In a previous work, we reported how the plasma electrical excitation frequency could influence the morphology of the films deposited by AP-DBD.[27] SEM observations and secondary ion mass spectrometry showed how the modulation of the electrical excitation prevents the formation of pinholes, particles and heterogeneities in the coatings. In the present work, the mean dissipated power density, which is known to influence the formation of particles,[42] was kept constant to 1.1 $W.cm^{-2}$ for both frequencies studied. However, the plasma gas current density (Figure 8) varied with the electrical excitation frequency. The maximum value of current density at 22 500 Hz (ca. 1.2 $mA.cm^{-2}$) was twice higher than the one measured at 10 000 Hz (ca. 0.6 $mA.cm^{-2}$). The current density variation, which is used to estimate the variation of plasma density according to discharge parameters, indicated the formation of a locally larger amount of active species at 22 500 Hz.[43] The higher concentration of active species and the high concentration of HMDSO lead to the formation of a higher density of particles at the highest plasma frequency, which increased the surface roughness.

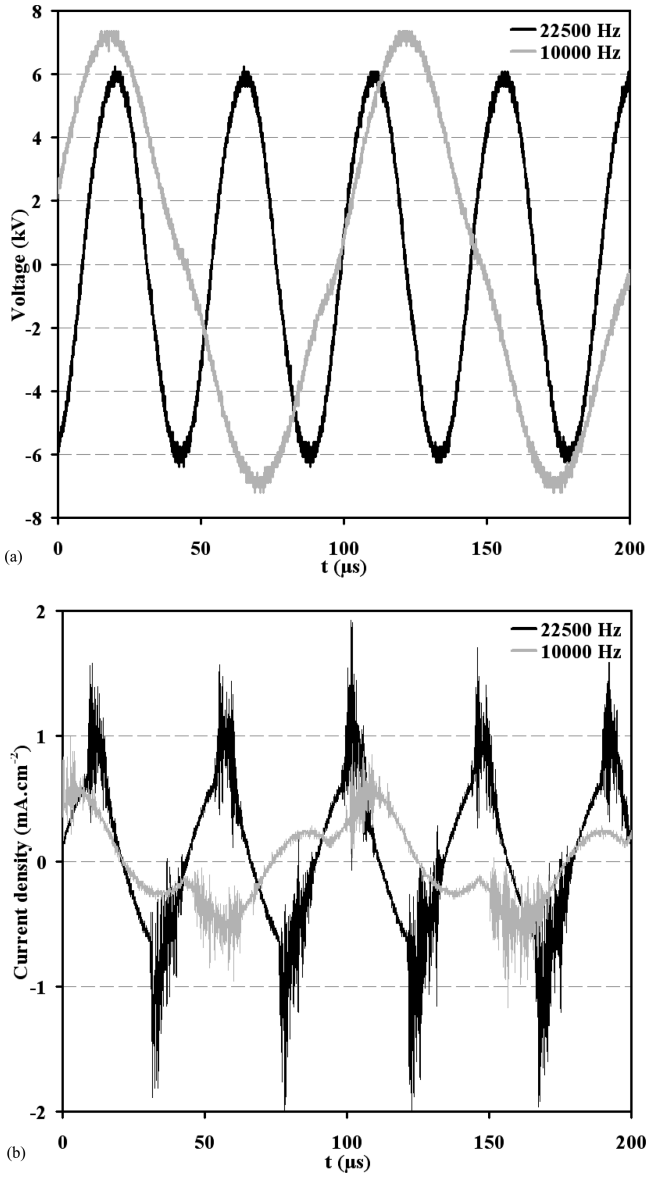

Figure 8. (a) Measured gas applied external voltage waveforms and (b) current density as a function of the plasma electrical excitation frequency.

4. CONCLUSIONS

Whereas previous methods adopted to achieve surfaces with both high water contact angle and high adhesion to water involve the use of fluorinated compounds or multistep processes, the formation of such surface using an atmospheric-pressure plasma single-step process without the presence of fluorine containing compounds was achieved. Thin films with high WCA and high WSA were prepared on aluminum foil by AP-DBD deposition of HMDSO. The technique, which is a way to quickly and simply prepare "sticky" high WCA surfaces, could be easily scaled up for large area. XPS and FTIR analyses showed the formation of ppHMDSO films with a high retention of hydrophobic pendant methyl groups, for all the plasma frequencies studied. SEM, AFM, and confocal microscopy showed some disparities in the morphology of the films and highlighted the importance of the micrometer and nanometer dual-scale roughness when targeting large water contact angles. The nanoscale roughness was achieved thanks to peculiar plasma deposition conditions, namely a high precursor concentration (1000 ppm) associated to a specific plasma excitation frequency (22 500 Hz). This new innovative surface, which was observed to be stable over a period of storage in air in excess of one year, could find applications in "lab on a chip" or microliter liquid handling devices for use in the life sciences where tiny quantities of liquid have to be hold in place without leaking or being contaminated by nearby materials. Moreover, the as-prepared surfaces exhibit high contact angle over a large pH range.

AUTHOR INFORMATION

Corresponding Author

*E-mail: nboscher@lippmann.lu.

Author Contributions

All authors have given approval to the final version of the manuscript.

Funding

This research was supported by the Luxembourgish "Fonds National de la Recherche" (FNR) through the TRASU Project.

Notes

The authors declare no competing financial interest.

The authors declare no competing financial interest.

■ ACKNOWLEDGMENTS

The authors thank the Luxembourgish "Fonds National de la Recherche" (FNR) for financial support through the TRASU Project. Dr. V. Vaché from Eurofoil, Dr. J. Guillot, S. François, Dr. T. Girot, Dr. R. Maurau, and A. Dembélé from CRP Gabriel Lippmann are hereby gratefully acknowledged for their skillful characterisations and valuable discussions.

■ REFERENCES

(1) Jin, M.; Feng, X.; Feng, L.; Sun, T.; Zhai, J.; Li, T.; Jiang, L. *Adv. Mater.* **2005**, *17*, 1977−1981.
(2) Cho, W. K.; Choi, I. S. *Adv. Funct. Mater.* **2008**, *18*, 1089−1096.
(3) Cassie, A. B. D.; Baxter, S. *Trans. Faraday Soc.* **1944**, *40*, 546−551.
(4) Wenzel, R. N. *Ind. Eng. Chem.* **1936**, *28*, 988−994.
(5) Saison, T.; Peroz, C.; Chauveau, V.; Berthier, S.; Sondergard, E.; Arribart, H. *Bioinspir. Biomim.* **2008**, *3*, 046004.
(6) Gao, L.; McCarthy, T. J. *Langmuir* **2006**, *22*, 2966−2967.
(7) Feng, L.; Zhang, Y.; Xi, J.; Zhu, Y.; Wang, N.; Xia, F.; Jiang, L. *Langmuir* **2008**, *24*, 4114−4119.
(8) Balu, B.; Berry, A. D.; Hess, D. W.; Breedveld, V. *Lab Chip* **2009**, *9*, 3066−3075.
(9) Boscher, N. D.; Carmalt, C. J.; Parkin, I. P. *J. Mater. Chem.* **2006**, *16*, 122−127.
(10) Yao, Y.; Dong, X.; Hong, S.; Ge, H.; Han, C. C. *Macromol. Rapid Commun.* **2006**, *27*, 1627−1631.
(11) Guo, Z.-G.; Liu, W.-M. *Appl. Phys. Lett.* **2007**, *90*, 223111−1−223111−3.
(12) Nicolas, M. *J. Colloid Interface Sci.* **2010**, *343*, 608−614.
(13) Zhao, X. D.; Fan, H. M.; Liu, X. Y.; Pan, H.; Xu, H. Y. *Langmuir* **2011**, *27*, 3224−3228.
(14) Peng, J.; Yu, P.; Zeng, S.; Liu, X.; Chen, J.; Xu, W. *J. Phys. Chem. C* **2010**, *114*, 5926−5931.
(15) Zhang, D.; Chen, F.; Yang, Q.; Yong, J.; Bian, H.; Ou, Y.; Si, J.; Meng, X.; Hou, X. *ACS Appl. Mater. Interfaces* **2012**, *4*, 4905−4912.
(16) Cho, K.-H.; Chen, L.-J. *Nanotechnology* **2011**, *22*, 445706−1−445706−14.
(17) Kim, D. S.; Lee, B.-K.; Yeo, J.; Choi, M. J.; Yang, W.; Kwon, T. H. *Microelectron. Eng.* **2009**, *86*, 1375−1378.
(18) Davies, J.; Haq, S.; Hawke, T.; Sargent, J. P. *Int. J. Adhes. Adhes.* **2009**, *29*, 380−390.
(19) Gao, L.; McCarthy, T. J. *J. Am. Soc. Chem.* **2006**, *128*, 9052−9053.
(20) Khorasani, M. T.; Mirzadeh, H.; Kermani, Z. *Appl. Surf. Sci.* **2005**, *242*, 339−345.
(21) Crick, C. R.; Parkin, I. P. *J. Mater. Chem.* **2009**, *19*, 1074−1076.
(22) Nwankire, C. E.; Favaro, G.; Duong, Q.-H.; Dowling, D. P. *Plasma Process. Polym.* **2011**, *8*, 305−315.
(23) Ji, Y.-Y.; Kim, S.-S.; Kwon, O.-P.; Lee, S.-H. *Appl. Surf. Sci.* **2009**, *255*, 4575−4578.
(24) Kim, M. C.; Klages, C.-P. *Surf. Coat. Technol.* **2009**, *204*, 428−432.
(25) Boscher, N. D.; Choquet, P.; Duday, D.; Verdier, S. *Surf. Coat. Technol.* **2011**, *205*, 5350−5357.
(26) Tendero, C.; Tixier, C.; Tristant, P.; Desmaison, J.; Leprince, P. *Spectrochim. Acta B* **2006**, *61*, 2−30.
(27) Boscher, N. D.; Choquet, P.; Duday, D.; Verdier, S. *Plasma Process. Polym.* **2010**, *7*, 163−171.
(28) Boscher, N. D.; Choquet, P.; Duday, D.; Verdier, S. *Surf. Coat. Technol.* **2010**, *205*, 2438−2448.
(29) Burkey, D. D.; Gleason, K. K. *J. Electrochem. Soc.* **2001**, *151*, F105−F112.
(30) Alexander, M. R.; Short, R. D.; Jones, F. R.; Michaeli, W.; Blomfield, C. J. *Appl. Surf. Sci.* **1999**, *137*, 179−183.
(31) O'Hare, L. A.; Hynes, A.; Alexander, M. R. *Surf. Interface Anal.* **2007**, *39*, 926−936.
(32) Azioune, A.; Marcozzi, M.; Revello, V.; Pireaux, J.-J. *Surf. Interface Anal.* **2007**, *39*, 615−623.
(33) Hoefnagels, H. F.; Wu, D.; de With, G.; Ming, W. *Langmuir* **2007**, *23*, 13158−13163.
(34) Nishino, T.; Meguro, M.; Nakamae, K.; Matsushita, M.; Ueda, Y. *Langmuir* **1999**, *15*, 4321−4323.
(35) Lafuma, A.; Quéré, D. *Nat. Mater.* **2003**, *2*, 457−460.
(36) Callies, M.; Quéré, D. *Soft Matter* **2005**, *1*, 55−61.
(37) Michael, N.; Bhushan, B. *Microelectron. Eng.* **2007**, *84*, 382−386.
(38) Trunec, D.; Navratil, Z.; Stahel, P.; Zajickova, L.; Bursikova, V. J.; Cech, V. J. *J. Phys. D: Appl. Phys.* **2004**, *37*, 2112−2120.
(39) Borra, J.-P. *J. Phys. D: Appl. Phys.* **2006**, *39*, R19−R54.
(40) Lee, J. H.; Kim, Y. S.; Oh, J. S.; Kyung, S. J.; Lim, J. T.; Yeom, G. Y. *J. Electrochem. Soc.* **2009**, *156*, D248−D252.
(41) Jidenko, N.; Jimenez, C.; Massines, F.; Borra, J.-P. *J. Phys. D: Appl. Phys.* **2007**, *49*, 4155−4163.
(42) Massines, F.; Gherardi, N.; Fornelli, A.; Martin, S. *Surf. Coat. Technol.* **2005**, *200*, 1855−1861.
(43) Choi, Y. H.; Kim, J. H.; Hwang, Y. S. *Thin Solid Film* **2006**, *506*, 389−395.